Microbial Pathogenesis 199 (2025) 107218

Contents lists available at ScienceDirect

Microbial Pathogenesis

journal homepage: www.elsevier.com/locate/micpath

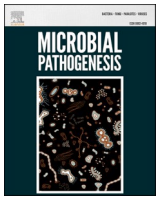

A novel genomic island encodes vibrioferrin synthesis in the marine pathogen *Photobacterium damselae* subsp. *damselae*

Beatriz Puentes [a], Alba Souto [b], Miguel Balado [a], Jaime Rodríguez [b,***], Carlos R. Osorio [a,**], Carlos Jiménez [b,****], Manuel L. Lemos [a,*]

[a] Department of Microbiology and Parasitology, Aquatic One Health Research Center (ARCUS), Universidade de Santiago de Compostela, Santiago de Compostela, 15782, Spain

[b] CICA-Centro Interdisciplinar de Química e Bioloxía, Departamento de Química, Facultade de Ciencias, Universidade da Coruña, A Coruña, 15071, Spain

ARTICLE INFO

Keywords:
Photobacterium damselae subsp. *damselae*
Siderophores
Vibrioferrin
Genomic islands
Virulence

ABSTRACT

In this study, we identified and analyzed a novel genomic island (GI), named *pdd*GI-1, located on chromosome II of certain strains of the marine pathogen *Photobacterium damselae* subsp. *damselae* (*Pdd*). This GI shares structural similarities with other GIs found in *Vibrio* species, such as the *Vibrio* seventh pandemic island-II (VSP-II) of *V. cholerae*. The *pdd*GI-1 island is a mosaic of gene blocks that encode functions related to ROS defense, anaerobic energy metabolism, and restriction-modification (RM) systems. Notably, *pdd*GI-1 also includes a complete vibrioferrin siderophore system, enabling the bacteria to thrive in low-iron environments. Vibrioferrin was chemically identified from cell-free supernatants of *Pdd* RG91. Additionally, a *pvsD* mutant deficient in vibrioferrin biosynthesis was generated and analyzed. The results suggest that *Pdd* strains harbouring *pdd*GI-1 gain a distinct growth advantage under iron-limited conditions. These findings, along with previous research, highlight the significant heterogeneity in iron assimilation systems among *Pdd* strains.

1. Introduction

Photobacterium damselae subsp. *damselae* (hereafter *Pdd*) is a marine bacterium that can behave as an opportunistic pathogen for many different marine animals, including mammals and even humans [1–3]. Strains of *Pdd* have been isolated from seawater, seaweeds, and seafood [4,5] and is commonly detected in the microbiota of fish farms [6], as well as in apparently healthy wild marine fish [7–9]. *Pdd* virulence relies mainly on extracellular products (ECPs), especially in a strong haemolytic activity [10–12]. The most relevant virulence factors described to date are damselysin, phobalysin P, and phobalysin C, haemolysins encoded by plasmid-borne *dly* and $hlyA_{pl}$ genes and chromosomal $hlyA_{ch}$ gene, respectively [13–15].

In most bacteria, one of the best established virulence factors is the ability to scavenge iron from the host by means of siderophores [16] or by using heme as iron source. In *Pdd*, the genes for heme uptake were previously characterized [17], but iron acquisition via siderophores is poorly studied [18]. In this regard, we previously demonstrated that some strains of *Pdd* can synthetize and use citrate as an effective iron-carrier [19]. In another study conducted with *Pdd* RG91, a strain not using citrate as siderophore, a proteomic analysis of iron-regulated proteins led to the identification of three proteins potentially involved in the synthesis and transport of a vibrioferrin-like siderophore [20]. The genes encoding these proteins were found in a subset of *Pdd* isolates in a genomic region containing mobile element-related genes, suggesting that they might have been acquired via horizontal gene transfer by certain *Pdd* lineages [21].

In this study, we identified the siderophore produced by *Pdd* RG91 as vibrioferrin and reported a complete set of genes involved in its synthesis and transport. These genes are located within the novel genomic island *pdd*GI-1, which exhibits a gene structure similar to some GIs found in Vibrios. The presence of *pdd*GI-1 enables a subset of *Pdd* isolates to

* Corresponding author.
** Corresponding author.
*** Corresponding author.
**** Corresponding author.
E-mail addresses: jaime.rodriguez@udc.es (J. Rodríguez), cr.osorio@usc.es (C.R. Osorio), carlos.jimenez@udc.es (C. Jiménez), manuel.lemos@usc.es (M.L. Lemos).

https://doi.org/10.1016/j.micpath.2024.107218
Received 8 October 2024; Received in revised form 3 December 2024; Accepted 8 December 2024
Available online 9 December 2024

produce and utilize the siderophore vibrioferrin.

2. Materials and methods

2.1. Bacterial strains, plasmids, and culture conditions

The bacterial strains used are listed in Table S1 and Table S2. *Pdd* strains (Table S1) were routinely grown at 25 °C on Tryptic Soy Agar (TSA) (Condalab) supplemented with 1 % NaCl (TSA-1) or in Tryptic Soy Broth (Condalab) supplemented with 1 % NaCl (TSB-1). *Escherichia coli* strains (Table S2) were routinely grown at 37 °C in Luria-Bertani (LB) broth or on LB agar (Condalab), supplemented with antibiotics when appropriate. Antibiotics were used at the following final concentrations: kanamycin (Km) at 50 μg/mL, ampicillin (Ap) sodium salt at 50 μg/mL, and rifampin (Rf) at 50 μg/mL.

2.2. Growth promotion and siderophore production assays

Growth promotion assays were conducted using 96-well microtiter plates. Each well contained 200 μL of CM9 medium [22] inoculated with a 1:50 dilution of an overnight culture of the *Pdd* strain in TSB-1 adjusted to an $OD_{600} = 0.5$. The medium was supplemented with either 10 mM $Fe_2(SO_4)_3$ for iron excess conditions, or 50 μM 2,2′-dipyridyl for iron-restricted conditions. Cultures were incubated at 25 °C with shaking at 150 rpm, and growth (OD_{600}) was recorded for 24 h using an iMACK Microplate reader (BioRad). Bacterial cultures grown in CM9 with 40 μM 2,2′-dipyridyl and an $OD_{600} \approx 0.8$ (after approximately 6 h of incubation) were used to obtain supernatants for measuring siderophore production using the chrome azurol-S (CAS) liquid assay [23]. For this purpose, equal volumes of CAS solution and supernatant were mixed, and the absorbance at 630 nm (A_{630}) was measured in a spectrophotometer (Hitachi U-2000) after 15 min of incubation at room temperature.

2.3. Detection of vibrioferrin by cross-feeding assays

Bioassays were designed to determine the production of vibrioferrin by *Pdd* isolates. *Vibrio alginolyticus* AR13, which utilizes vibrioferrin as an iron source but does not produce it [24], was used as the indicator strain. This strain was inoculated into CM9 minimal medium containing the iron chelator 2,2′-dipyridyl at 150 μM, a concentration above the minimal inhibitory concentration. *Pdd* RG91 wild type, the RG91 *pvsD* defective mutant, and all other tested strains were cultured on TSA-1 plates. Bacterial cells were then harvested with a sterile loop and placed on top of the indicator strain plates. The results were considered positive when a growth halo of the indicator strain, indicative of vibrioferrin production, was observed around the discs. A blank disc containing 10 μL of a 10 μM $Fe_2(SO_4)_3$ solution was used as a positive control for growth.

2.4. Sequencing of Pdd RG91 genome

Genomic DNA from *Pdd* RG91 was purified using the GNOME DNA kit (Q-biogene) and sequenced on an Illumina MiSeq sequencer with 100 × coverage. The reads were trimmed for quality, adapter sequences, and ambiguous nucleotides, and were assembled using SPAdes 3.6 [25]. The resulting draft genome sequences were annotated and compared with the Rapid Annotations using Subsystems Technology (RAST) Server [26]. This Whole Genome Shotgun project has been deposited at DDBJ/ENA/GenBank under the accession JBHDUS000000000. The version described in this paper is version JBHDUS010000000.

2.5. Detection by PCR of ppdGI-1 genetic markers

A PCR-based screening of *Pdd* strains from various geographical origins and hosts (Table S1) was performed to assess the prevalence of *ppd*GI-1, using primers listed in Table S3. DNA extractions were performed with InstaGene™ Matrix (Bio-Rad), and PCR reactions were carried out using NZYTaq II 2x Green Master Mix (NZYTech), following the manufacturer instructions. A 2 % agarose gel was used to analyze the amplified PCR products.

2.6. Construction of a pvsD mutant in Pdd RG91

The *pvsD* gene, which encodes a vibrioferrin biosynthesis enzyme, was deleted by allelic exchange with the Km^r suicide vector pNidkan derived from pCVD442, as previously described [27]. Briefly, a non-functional allele of *pvsD* was constructed by PCR amplification of the amino- and carboxy-terminal regions, which were then fused to create an in-frame deletion of 90 % of the *pvsD* internal coding sequence. The resultant plasmid, containing the truncated allele, was transferred from *E. coli* S17-1-λpir into a rifampin-resistant derivative of the RG91 strain. Selection for plasmid integration was performed using Rf and Km, followed by selection for a second recombination event using sucrose resistance (15 % w/v). Primers used for mutant construction are shown in Table S3.

2.7. Detection of siderophore vibrioferrin by mass spectrometry (MS) and absorption spectroscopy (UV)

Siderophore detection in liquid media was performed using cell-free supernatants from cultures of *Pdd* RG91, grown at 25 °C in 1 L flasks containing CM9 minimal medium supplemented with 40 μM 2,2′-dipyridyl, with continuous shaking at 150 rpm for 24 h. The flasks were inoculated with 20 mL of a fresh *Pdd* culture in TSB-1. When the bacterial cultures reached an OD_{600} of 0.8, the cells were removed by centrifugation at 10 000×*g* for 10 min, and the supernatants were filtered through a 0.45 μm pore-size membrane using a continuous filtration cartridge (Millipore).

One liter of cell-free culture supernatant was stored at −20 °C and then lyophilized, yielding 2.789 g of solid material, which was divided into several portions for subsequent analysis. A first portion (215.9 mg) was dissolved in 1 mL of 0.1 % TFA and subjected to solid-phase extraction (SPE) using a pre-activated Oasis MCX cartridge (1 g sorbent, Waters). The cartridge was first eluted with 10 mL of 0.1 % TFA (PDMCX1 fraction) followed by 10 mL of H_2O:MeOH (1:1) each containing 0.1 % TFA (PDMCX2 fraction), 10 mL of MeOH (PDMCX3 fraction), and finally with 10 mL of H_2O: 7N NH_3 in MeOH (2:1) (PDMCX4 fraction). These fractions were lyophilized yielding 21.5 mg (PDMCX1), 21.9 mg (PDMCX2), 4.4 mg (PDMCX3), and 11.1 mg (PDMCX4). The CAS test for Fe^{3+}-complexing substances and siderophore activity analysis revealed that PDMCX1 was the most active fraction. The active lyophilized siderophore fraction, PDMCX1, was extracted with MeOH to remove salt compounds, yielding two subfractions after lyophilization: PDMCX1-MeOH (3.8 mg) and PDMCX1-salts (4.8 mg) (Fig. S1).

The PDMCX1-MeOH subfraction, which tested positive in the CAS test and the siderophore activity assay, was analyzed by LC-DAD-MS under the following conditions: Atlantis dC18 column (100 × 4.6 mm, 5 μm) (Waters) with a mobile phase consisting of a 35 min gradient from 10 to 100 % CH_3CN in H_2O (v/v), then 5 min at 100 % CH_3CN, and finally 10 min from 100 % to 10 % CH_3CN/H_2O (v/v), at a flow rate of 1 mL/min. All measurements were performed on an ESI ion trap mass spectrometer LTQ-Orbitrap Discovery in negative mode attached to an Accela HPLC system (Thermo-Fisher Scientific). Accurate mass measurements were taken using the FT-MS Orbitrap module at a resolution >30 000 FWHM (full width at half maximum) for obtaining elemental composition of the $[M - H]^-$ ion adduct within 1–3 ppm accuracy.

The TIC-HPLC chromatogram of the PDMCX1-MeOH fraction (Fig. S2B) showed two peaks eluting at $R_t = 2.49$ and $R_t = 3.89$–4.01 min, which were named PDMCX1-MeOH-H1 and PDMCX1-MeOH-H2 HPLC fractions, respectively. The UV spectrum of PDMCX1-MeOH-H1

HPLC fraction, eluted at R_t = 2.49 min, displayed an end absorption band at $\lambda \approx 200$ nm (Fig. S2C), while its corresponding MS (Fig. S2E) showed the [M − H]$^-$ ion adduct at *m/z* 433.1099 (calculated for $C_{16}H_{21}N_2O_{12}^-$, *m/z* 433.1100) that matched that of free vibrioferrin (VF, *apo*vibrioferrin, **1**). The HPLC fraction PDMCX1-MeOH-H2, eluted at R_t = 3.89–4.01 min, displayed the presence of a compound with an UV spectrum with an end absorption band at $\lambda \approx 258$ nm (Fig. S2D) and a MS (Fig. S2F) showing the [M − H]$^-$ ion adduct at *m/z* 441.0953 (calculated for $C_{16}H_{18}BN_2O_{12}^-$, *m/z* 441.0958) that matched that of borate-vibrioferrin complex (B-VF complex, **2**).

Chelation test and analytical detection of vibrioferrin-Fe(III) and vibrioferrin-Ga(III) complexes. A second portion of the lyophilized material (373.0 mg) was subjected to the same procedure as previously described, yielding the methanol fraction PDMCX1-MeOH. This fraction was divided into two portions, which were separately transferred into two vials, to which a small amount of $FeCl_3{\cdot}6H_2O$ or $GaBr_3$ (~1 mg) was added, resulting in two subfractions named PDMCX1-MeOH-Fe and PDMCX1-MeOH-Ga, respectively. In both cases, a turbidity was observed after metal salt addition. Each subfraction was analyzed by HPLC-DAD-MS under the same conditions previously described. Iron complex of vibrioferrin was detected by HPLC-DAD-MS analysis of the PDMCX1-MeOH-Fe subfraction in the chromatographic peak eluted at R_t = 2.49 min (Figs. S3A and S3B). The UV spectrum exhibited a shoulder around 300 nm, consistent with a ligand-to-metal ion charge-transfer band, typical of ferric complexes [28] and the HRMS analysis displayed the [M − H]$^-$ ion adduct at *m/z* 486.0210 (calculated for $C_{16}H_{18}FeN_2O_{12}^-$, *m/z* 486.0209) that matched that of iron-vibrioferrin complex (Fe-VF complex, **3**) (Figs. S3C and S3D). HPLC-DAD-MS analysis of subfraction PDMCX1-MeOH-Ga revealed a peak at R_t = 1.90 min, which was identified as the gallium complex of vibrioferrin (**4**) (Figs. S4A and S4B). HRMS analysis revealed the presence of the [M − H]$^-$ ion adduct at *m/z* 499.0111 (calculated for $C_{16}H_{18}GaN_2O_{12}^-$, *m/z* 499.0121), corresponding to the gallium-vibrioferrin complex. Its UV spectrum further confirmed the presence of this complex (Figs. S4C and S4D).

2.8. Assays of virulence for fish

Virulence assays were conducted using turbot (*Scophthalmus maximus*) fingerlings with an average weight of 15 g, divided into two groups of 30 fish per strain tested. The inocula were prepared by suspending several colonies from a 24-h TSA-1 culture in saline solution to achieve an OD_{600} of 0.5. Turbot fingerlings were inoculated intraperitoneally (IP) with 0.1 mL of the bacterial suspension. The actual concentration of injected bacteria, determined by plate count on TSA-1, was between 2 and 4 × 10^4 bacterial cells per fish. Mortalities were recorded daily for 10 days post-injection, and the statistical significance of survival differences among *Pdd* strains was assessed using the Kaplan-Meier method and a log-rank test in SPSS 25 (SPSS for Windows, version 25).

All experiments involving fish were conducted in strict accordance with the guidelines established by the European Union (2010/63/UE) and the Spanish legislation (RD 53/2013) for the use of animals in research. All fish were anesthetized with tricaine methanesulfonate (MS-222) at 80 mg L^{-1} before IP injection, and survivors were euthanized at the conclusion of the experiments with a MS-222 overdose of 160 mg L^{-1}. The procedure was authorized by the Bioethics Committee of the University of Santiago de Compostela (approved protocol No. 15004/14/003).

3. Results and discussion

3.1. Genome sequence analysis of Pdd RG91 and pddGI-1 general features

In a previous proteomics study of *Pdd* RG91 [20], we identified three proteins involved in the synthesis (PvsD) and transport (PvuA and PsuA) of the siderophore vibrioferrin [29,30]. These *Pdd* RG91 proteins were found to be upregulated when the strain was cultivated under low-iron conditions. To identify and characterize the genomic region encoding these proteins, we sequenced and analyzed the genome of *Pdd* RG91 in this study.

A comparative in silico analysis between the genome sequence of *Pdd* RG91 and other *Pdd* genomes available in GenBank revealed that chromosome II of RG91 harbours unique sequences homologous to those previously reported for the synthesis and transport of vibrioferrin in *Vibrio parahaemolyticus* [29]. A pairwise comparison between the RG91 genome (GenBank Acc. No. JBHDUS000000000) and that of *Pdd* ATCC33539 (Acc. No. ADBS00000000), a strain lacking homologues for siderophore genes (including both the vibrioferrin gene cluster and related sequences), clearly shows that the RG91 genome contains a region encoding a complete vibrioferrin-like siderophore system (Fig. 1). Notably, this region is located within a novel genomic island (GI), which we have named *pdd*GI-1. The predicted functions of the ORFs found within this GI are presented in Table S4.

GI *pdd*GI-1 is located within a variable region of chromosome II (Fig. 1) and is flanked by two conserved genes: a fructose transporter component C (locus VDA_000334 in the ATCC33539 genome annotation) and a serine tRNA, along with a hypothetical protein (locus VDA_000337). The backbone of *pdd*GI-1 is primarily composed of phage-related proteins, whose homologues are present in other well-described GIs (Table S4). Notably, *orf1* and *orf35* encode two prophage-related proteins that show significant homology to integrases and AlpA-type regulatory proteins found in numerous *Vibrio*, *Photobacterium*, and *Pseudomonas* genomes, with amino acid similarity ranging from 78 to 81 %. It is noteworthy that the integrase (*orf1*) located at the 5′ end of *pdd*GI-1, the hypothetical proteins *orf23-25* located internally, and *orf39-40* located at the 3′ end, exhibit significant homology to proteins encoded by the *Vibrio cholerae* seventh pandemic island-II (VSP-II), which is related to the epidemiological success of this pandemic clone [31], and by the VVI-II genomic island characterized in *V. vulnificus* [32] (Fig. 1B). Additionally, some *V. anguillarum* and *P. phosphoreum* genomes contain GIs, not yet characterized, that include integrase homologues closely related to *orf35* and *36* in *V. anguillarum* and *orf35-40* in *P. phosphoreum* (Fig. 1B). These findings suggest that these genes are commonly present in DNA structures of other GIs and likely constitute the backbone of this family of GIs. Moreover, the presence of homologues in many bacterial species indicates that this family of accessory genetic elements is widespread among marine bacteria.

Horizontally acquired genes can provide recipient strains with selective advantages and virulence factors, potentially leading to new pathogens [33]. *pdd*GI-1 contains three transposases (*orf2, orf9, orf21*) and genes associated with ROS defense, anaerobic energy metabolism, restriction-modification (RM) systems, and a complete vibrioferrin iron uptake system. These features may confer benefits to the host.

orf4 encodes a 179-aa protein with a YciW domain (COG2128), typical of peroxidase-related enzymes. Its closest homologues in *Vibrionaceae* have 78–81 % similarity, suggesting a role in antioxidant defense against reactive oxygen species produced by host immune cells [34]. *orf6* to *orf8* are homologous to *dmsABCD* genes, which encode enzymes for anaerobic respiration with N- and S-oxide acceptors like DMSO and TMAO. DmsA and DmsB form a catalytic dimer anchored by DmsC, while DmsD exports DmsA to the TAT translocon [35,36]. These reductases are prevalent in *Vibrionaceae* and support respiration in low-oxygen environments, aiding host colonization [37,38]. TMAO, found in marine environments and animal tissues, is used as an osmolyte [39]. The presence of a duplicate *dms* operon in RG91, sharing 52–81 % similarity with *pdd*GI-1, suggests that TMAO reduction is crucial for *Pdd* ecology. The versatility in metabolic systems within *Vibrionaceae* species enables adaptation to varying environmental conditions.

Both phage-like elements and genomic islands (GIs) often contain selfish DNA, including restriction-modification (RM) systems that

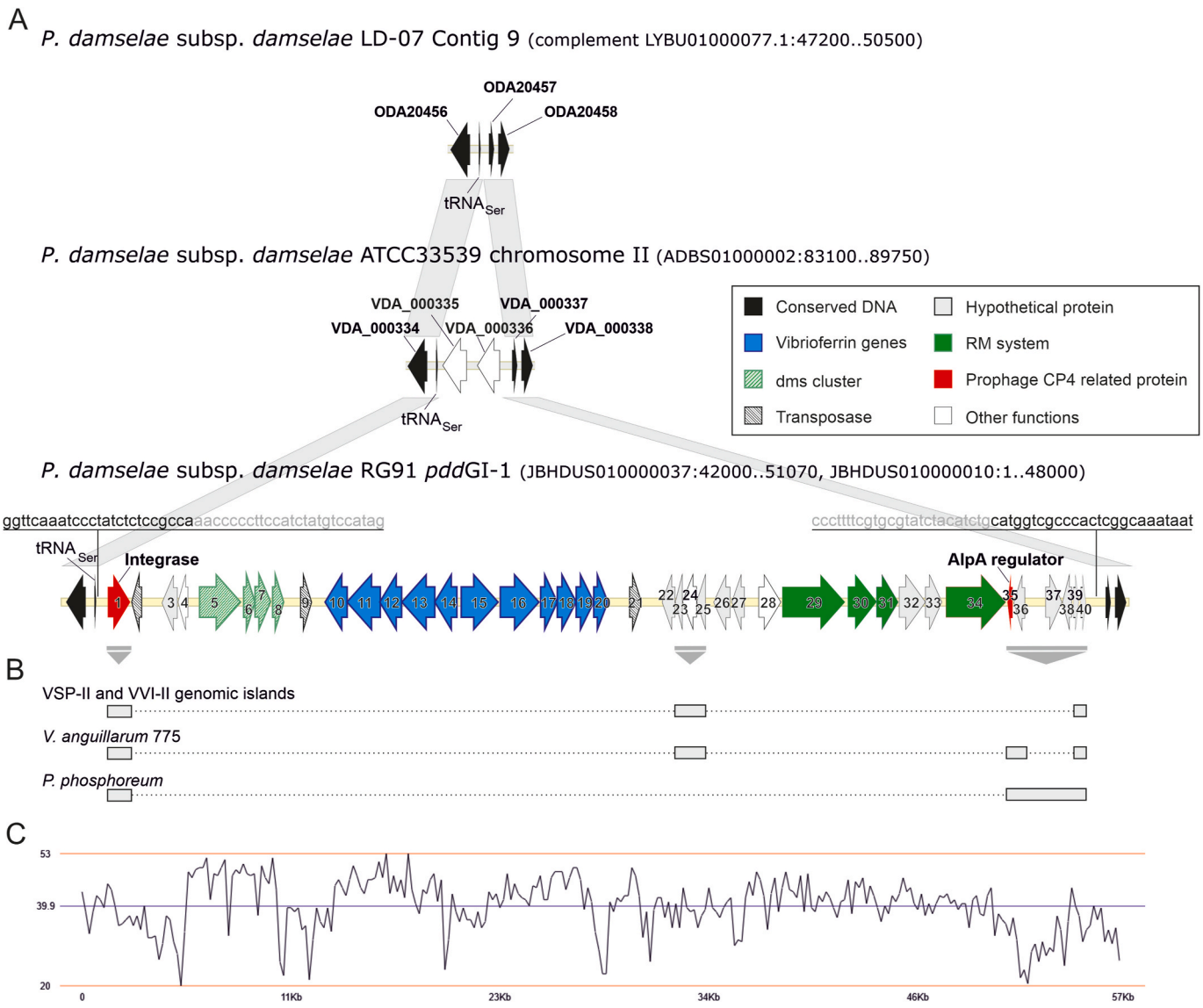

Fig. 1. Gene arrangement of the *Pdd* RG91 genomic island *pdd*GI-1. (A) Alignment of *pdd*GI-1 sequence and the flanking chromosomal region (GenBank access No. JBHDUS010000037: 42000 … 51070 and JBHDUS010000010: 1 … 48000) with the genomic sequences of *Pdd* LD-07 (GenBank access No. LYBU01000077:47200 … 50500) and *Pdd* ATCC33539 (GenBank access No. ADBS01000002: 83100 … 89750). Grey blocks indicate identical sequences. (B) Distribution of BlastP homologues associated with other genomic island backbones on the *pdd*GI-1 sequence. Multiple alignments with the same database sequence are connected by a dotted line. (C) GC content distribution of *pdd*GI-1.

ensure their persistence [33]. *orf29* and *orf30* encode a Type I RM system with restriction and methylase subunits. These genes have close homologues in *Photobacterium angustum* S14 (97–99 % amino acid identity) and several *Vibrio* species, including *V. parahaemolyticus*, *V. harveyi*, and *V. cholerae*, with over 80 % similarity (data not shown). *orf31* encodes a specificity subunit of a Type I RM system with homologues in *V. cholerae*, while *orf 34* shows 97 % similarity to a Type III restriction endonuclease from *V. harveyi*. Although RM systems are not unique to *pdd*GI-1—as mobile genetic elements commonly harbor them and over 80 % of bacterial genomes contain multiple RM systems [40]—they can provide a significant selective advantage by protecting against environmental bacteriophages [41].

As shown, all genes in *pdd*GI-1 have close homologues in various marine bacterial species, indicating that these genes are part of a variable gene pool within the marine microbiota. Interestingly, although the mean GC content of *pdd*GI-1 is similar to that of the rest of chromosome II (39.9 % vs. 39.6 %, respectively), specific sequence blocks within *pdd*GI-1 have GC content patterns identical to those in related GIs from other vibrios [32,42]. Notably, the distribution of GC content within *pdd*GI-1 shows breaks that correlate with the distribution of homologues (Fig. 1C). Consequently, the genes can be grouped into blocks based on homologues distribution, functional relationships, and GC content (Fig. 1C). These findings suggest that *pdd*GI-1 likely originated from successive gene acquisition events from other *Vibrionaceae* rather than from an ancient association with *Pdd*.

3.2. *pddGI-1 harbours genes encoding vibrioferrin synthesis and transport*

Notably, *pdd*GI-1 contains a complete vibrioferrin iron uptake system (*orf17-orf26*) with 80–99 % amino acid similarity to vibrioferrin system in *V. harveyi* (Table S4), maintaining the same gene organization (Fig. 1A). This system includes two operons transcribed from divergent promoters: one operon (*pvsABDE*) encodes biosynthesis functions [30], while *pvsC* encodes the siderophore exporter. The second operon consists of genes for ferric-vibrioferrin uptake (*pvuA1, pvuA2, pvuBCDE*), where *pvuA1* and *pvuA2* are outer membrane receptors and *pvuBCDE*

forms the ABC transport system for iron-siderophore transport through the inner membrane [29,43,44].

Siderophores are compounds synthesized by microorganisms to solubilize iron extracellularly and transport it into cells through specific transporters. Thus, the ability to produce and utilize a siderophore is crucial for forming natural marine bacterial communities [45] and is often essential for virulence [46]. Vibrioferrin, originally identified in Vibrios such as *V. parahaemolyticus, V. alginolyticus*, and *V. splendidus* [28], is also found in many marine bacteria [47], including numerous environmental *Vibrio* species [45] and other genera like *Marinobacter* [48] and *Edwardsiella* [49], highlighting its widespread presence in marine bacteria. It has been proposed that the distinctive properties of vibrioferrin may play a crucial role in enhancing iron bioavailability through photoredox reactions in marine environments [47].

3.3. Production of vibrioferrin by Pdd RG91

The identification of vibrioferrin-related proteins under low-iron conditions [20] and the presence of genes involved in vibrioferrin synthesis and transport in *Pdd* RG91 strongly suggest that this strain produces vibrioferrin as its siderophore. To confirm this, we generated an RG91 mutant lacking most of the *pvsD* coding sequence, essential for vibrioferrin biosynthesis [30]. We then conducted biological assays to compare the wild-type and mutant strains.

Both strains exhibited similar growth under iron-excess conditions (Fig. 2). However, under iron-restricted conditions, the *pvsD* mutant showed a 40 % reduction in growth compared to the parental strain, which reached an OD_{600} of approximately 1.4 (Fig. 2B). Cross-feed bioassays with *V. alginolyticus* AR13, an indicator strain that uses vibrioferrin as an iron source but does not produce it [24], showed that the RG91 parental strain promoted its growth under iron deficiency, whereas the *pvsD* mutant did not (Fig. 2A).

These results suggest that *Pdd* RG91 produces vibrioferrin. To confirm this hypothesis, cell-free culture supernatants of RG91, obtained under low iron conditions, were subjected to Solid Phase Extraction (SPE) using Oasis MCX cartridges, resulting in several fractions (PDMCX1-X4) that were then tested using the CAS assay and siderophore activity assays (Fig. S1). To verify the presence of vibrioferrin, the CAS-positive and siderophore-active fraction PDMCX1 was desalted through MeOH extraction, yielding the subfractions PDMCX1-MeOH and PDMCX1-salts, which were subsequently analyzed by LC-DAD-MS (Fig. 3A and Figs. S2–S4).

Thus, the extracted mass chromatogram (*m/z* 400.00–450.00) of the desalted PDMCX1 subfraction (Fig. 3B) revealed the presence of two compounds with retention times of 2.49 and 4.01 min. Their corresponding high-resolution mass spectra displayed the $[M-H]^-$ ion adducts at *m/z* 433.1099 (calculated for $C_{16}H_{21}N_2O_{12}^-$, *m/z* 433.1100) (Fig. 3C) and at *m/z* 441.0953 (calculated for $C_{16}H_{18}BN_2O_{12}^-$, *m/z* 441.0958) (Fig. 3D), which matched those of *apo*vibrioferrin (VF, **1**) and its boron complex (B-VF, **2**), respectively. Furthermore, the UV spectrum of each compound exhibited maximum absorption bands at 201 nm and 258 nm (Fig. S5), corresponding to those reported for vibrioferrin and its boron complex, respectively [28].

To corroborate the presence of vibrioferrin, a chelation test and analytical detection of vibrioferrin-metal complexes were conducted (Fig. 3E–H). The active PDMCX1-MeOH subfraction was mixed with small amounts of $FeCl_3{\cdot}3H_2O$ or $GaBr_3$. The resulting products were then analyzed using HPLC-DAD-HRMS following the same procedures employed previously (Fig. S1). As a result, the iron complex of vibrioferrin (Fe-VF, **3**) was identified in the analysis of the PDMCX1-MeOH-Fe subfraction by the presence of the $[M-H]^-$ ion adduct at *m/z* 486.0210 (calculated for $C_{16}H_{18}FeN_2O_{12}^-$, *m/z* 486.0209) that matched that of the iron complex of vibrioferrin (Fe-VF, **3**) (Fig. 3E and G).

HPLC-DAD-HRMS analysis of the PDMCX1-MeOH subfraction, after addition of $GaBr_3$, revealed the presence of the corresponding gallium complex of vibrioferrin (Ga-VF, **4**) at $R_t = 1.90$ min, showing the $[M-H]^-$ ion adduct at *m/z* 499.0111 (calculated for $C_{16}H_{18}GaN_2O_{12}^-$, *m/z* 499.0121) (Fig. 3F and H). In both cases, the characteristic iron isotopic distribution of each metal was observed. Collectively, these results unambiguously confirm that *Pdd* RG-91 produces the siderophore vibrioferrin.

As anticipated, vibrioferrin was undetectable in the culture supernatants of the RG91 *pvsD* mutant (data not shown). Interestingly, the *pvsD* mutant exhibited a weaker CAS-positive reaction, suggesting the potential production of other siderophore-active molecules by this strain (see below). These findings together confirm that *pddGI-1* contains an active vibrioferrin gene cluster, which likely provides a selective advantage to *Pdd* strains that harbor it.

3.4. Distribution of pddGI-1 in a collection of Pdd strains

To investigate the distribution of *pdd*GI-1 among various *Pdd* isolates, we analyzed gene block linkage and intra-GI variability. We performed PCR amplification on 41 *Pdd* strains to detect the presence of seven specific genes (Table S1). Four key genes were targeted: integrase (*orf1*), the vibrioferrin biosynthesis gene (*pvsD*), the *dms* cluster (*dmsC*), and the RM system (*orf32*). Additionally, we checked for the presence of genes VDA_0334 and VDA_0337, which flank the insertion site of *pdd*GI-1 (Fig. 1), as well as genes VDA_0335 and VDA_0336, which replace *pdd*GI-1 in the *Pdd* ATCC33539 genome (Fig. 1). PCR results of 17

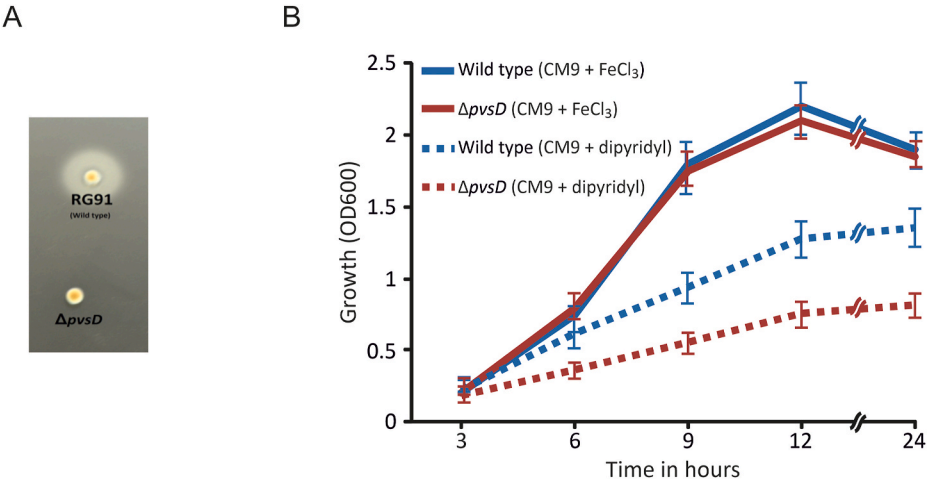

Fig. 2. (A) Cross-feeding assay of *Pdd* RG91 and its derivative mutant defective in *pvsD* to detect vibrioferrin production using *V. alginolyticus* AR13 as indicator strain. (B) Growth under iron excess and iron deficient conditions of wild type strain and its *pvsD* defective mutant.

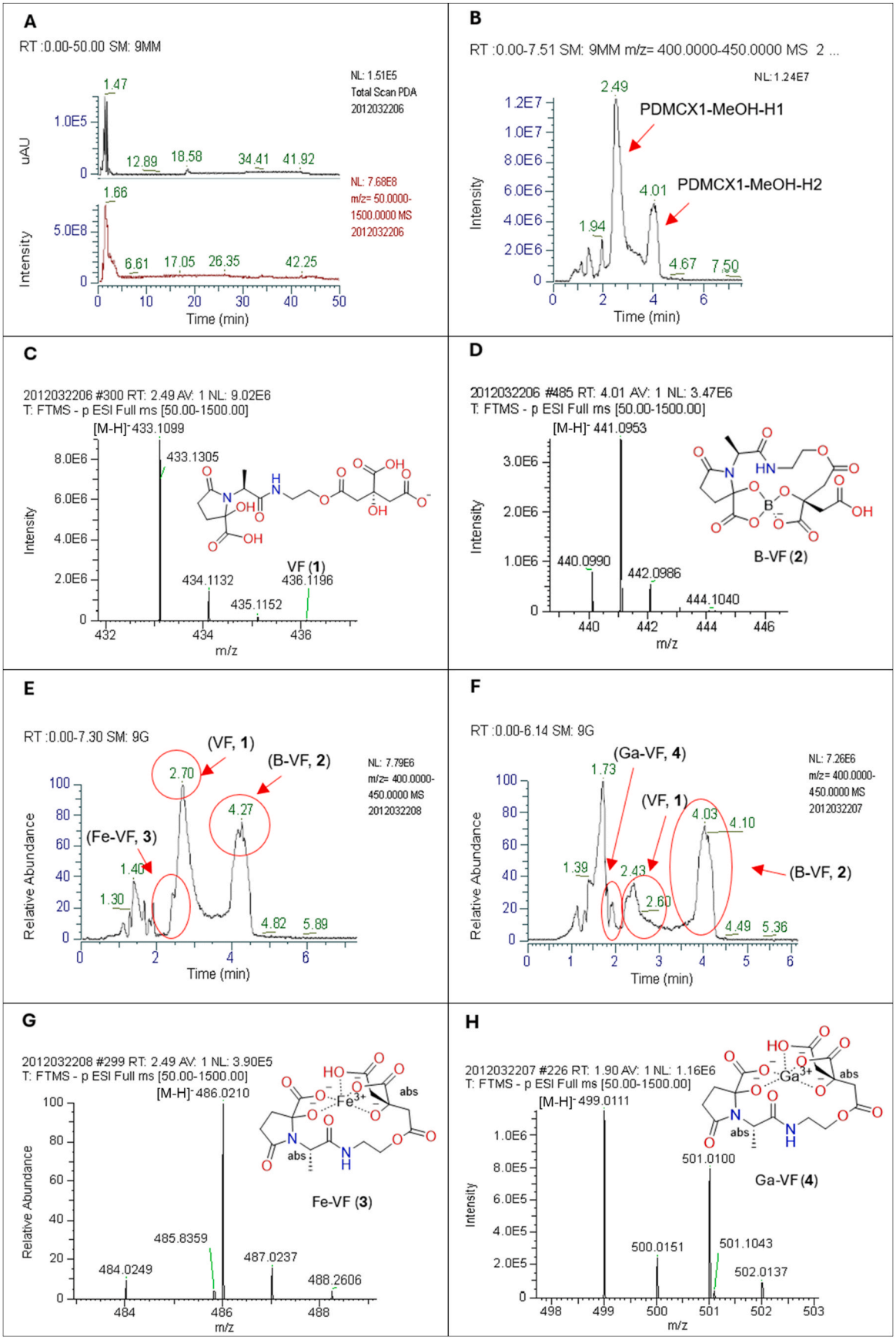

(caption on next page)

Fig. 3. (**A**) HPLC-DAD-HRMS chromatogram of the desalted PDMCX1-MeOH subfraction. (**B**) Extracted mass chromatogram (*m/z* 400.00–450.00). (**C**) High-resolution mass spectrum (HRMS) of the peak at 2.49 min (PDMCX1-MeOH-H1) indicating the presence of *apo*vibrioferrin (VF, **1**). (**D**) HRMS of the peak at 4.01 min (PDMCX1-MeOH-H2) indicating the presence of the borate vibrioferrin complex (B-VF, **2**). (**E**) Extracted mass chromatogram (*m/z* 400.00–450.00) of HPLC-HRMS chromatogram of PDMCX1-MeOH subfraction after addition of $FeCl_3{\cdot}3H_2O$. (**F**) Extracted mass chromatogram (*m/z* 400.00–450.00) of PDMCX1-MeOH subfraction after addition of $GaBr_3$. (**G**) (−)-HRESIMS of PDMCX1-MeOH-Fe displaying the $[M - H]^-$ ion at *m/z* 486.0210 of iron vibrioferrin complex (Fe-VF, **3**) (calcd. For $C_{16}H_{18}FeN_2O_{12}^-$, *m/z* 486.0209). (**H**) (−)-HRESIMS of PDMCX1-MeOH-Ga displaying the $[M - H]^-$ ion at *m/z* 499.0111 of gallium vibrioferrin complex (Ga-VF, **4**) (calcd. For $C_{16}H_{18}GaN_2O_{12}^-$, *m/z* 499.0121).

representative strains are summarized in Table 1.

The results showed that 11 out of 41 strains tested carry the *pdd*GI-1 element, as indicated by the presence of at least the integrase, *dmsC*, and *pvsD* genes. This suggests that *pdd*GI-1 is prevalent among a significant subset of *Pdd* isolates. There is no correlation between the presence of *pdd*GI-1 and the origin of the strains. However, intra-*pdd*GI-1 variability was observed, with two of the 11 positive strains lacking amplification for the RM system component (*orf32*) (Table 1). This variability supports the notion that *pdd*GI-1 elements may have arisen through gene block recruitment. While all strains tested positive for the genes flanking the *pdd*GI-1 insertion site (VDA_000334 and VDA_000337), only the ATCC33539 strain was positive for VDA_000335 and VDA_000336 (data not shown). Furthermore, all strains positive for *pdd*GI-1 also showed positive results in a PCR targeting the region between VDA_0334 and *orf1* (Table 1), suggesting that all *pdd*GI-1 elements are inserted at the same genomic location. These findings are consistent with the alignment of the RG91 *pdd*GI-1 element and its flanking regions with genome sequences available in GenBank (Fig. 1).

3.5. Vibrioferrin production in different Pdd strains

To assess vibrioferrin production in *Pdd* strains harbouring *pdd*GI-1, cross-feed bioassays were performed using *V. alginolyticus* AR13 as the indicator strain. *Pdd* RG91 and its *pvsD* mutant were used as positive and negative controls, respectively. All strains containing *pdd*GI-1 successfully promoted the growth of *V. alginolyticus* AR13, whereas strains lacking this element did not (Table 1). These findings confirm that all *pdd*GI-1-like elements possess an active vibrioferrin gene cluster, and that having *pdd*GI-1 enables the bacteria to produce vibrioferrin.

Additionally, the role of vibrioferrin production in bacterial growth under low iron conditions was investigated. *Pdd* strains with *pdd*GI-1 were tested for their growth under both iron-rich and iron-poor conditions, and siderophore production was measured using the CAS assay.

Strains of *Pdd* carrying *pdd*GI-1 exhibited significantly higher growth yields and siderophore production under low-iron conditions compared to strains lacking this element (Fig. 4). Notably, all *pdd*GI-1-harbouring strains showed a phenotype almost identical to that of the RG91 strain. In contrast, strains without *pdd*GI-1 displayed reduced siderophore production and lower growth yields, similar to the RG91 *pvsD* null mutant. The ATCC33539 strain had the lowest growth rate and siderophore production among all tested strains. These findings suggest that vibrioferrin production provides a growth advantage under iron-limited conditions, supporting the hypothesis that vibrioferrin may play a role in *Pdd* virulence.

Notably, the RG91 strain had a CAS assay value of −0.8, reflecting high siderophore production, whereas the *pvsD* mutant had a lower value of −0.6 (Fig. 4), similar to strains lacking *pdd*GI-1. This CAS value suggests that the mutant still produces siderophores, albeit at lower levels, potentially indicating the presence of an alternative siderophore. Since RG91 does not use citrate as a siderophore [19], the mutant's lower CAS value may indicate the production of an alternative, unidentified siderophore. The production of multiple siderophores likely offers a growth advantage and increased adaptability in low-iron environments [50].

Table 1
Detection of *pdd*GI-1 markers by PCR and vibrioferrin production in a subset of representative *Pdd* strains. The complete set of strains tested is shown in Table S1

Strain	Isolation source	*pdd*GI-1 markers							Vibrioferrin production
		Integrase (*orf1*)	*dmsC* (*orf 7*)	*pvsD* (*orf 11*)	RM system (*orf32*)	VDA_334 - *orf1* linkage	VDA_000334	VDA_000337	
ATCC33539	*Chromis punctipinnis* (USA)	—	—	—	—	—	+	+	—
ATCC35083	*Carcharhinus plumbeus* (USA)	—	—	—	—	—	+	+	—
RG91	*Scophthalmus maximus* (Spain)	+	+	+	+	+	+	+	+
LD07	*Sparus aurata* (Spain)	—	—	—	—	—	+	+	—
RM71	*Scophthalmus maximus* (Spain)	—	—	—	—	—	+	+	—
9FT1M3	*Carcharhinus plumbeus* (USA)	+	+	+	-	+	+	+	+
CDC2227–81	Human	—	—	—	—	—	+	+	—
RG214	*Scophthalmus maximus* (Spain)	+	+	+	+	+	+	+	+
H22060601R	*Pagrus auriga* (Spain)	+	+	+	+	+	+	+	+
H01100403D1	*Pagrus auriga* (Spain)	+	+	+	—	+	+	+	+
H29060602R	*Pagrus auriga* (Spain)	+	+	+	+	+	+	+	+
ACR208.1	*Scophthalmus maximus* (Spain)	+	+	+	+	+	+	+	+
AQP16.1	*Scophthalmus maximus* (Spain)	—	—	—	±	—	+	+	—
VIRO-RIÑÓN	*Scophthalmus maximus* (Spain)	+	+	+	+	+	+	+	+
AZ247.1	*Scophthalmus maximus* (Spain)	+	+	+	+	+	+	+	+
AZ245.1	*Scophthalmus maximus* (Spain)	+	+	±+	+	+	+	+	+
RG153	*Scophthalmus maximus* (Spain)	+	+	+	+	+	+	+	+

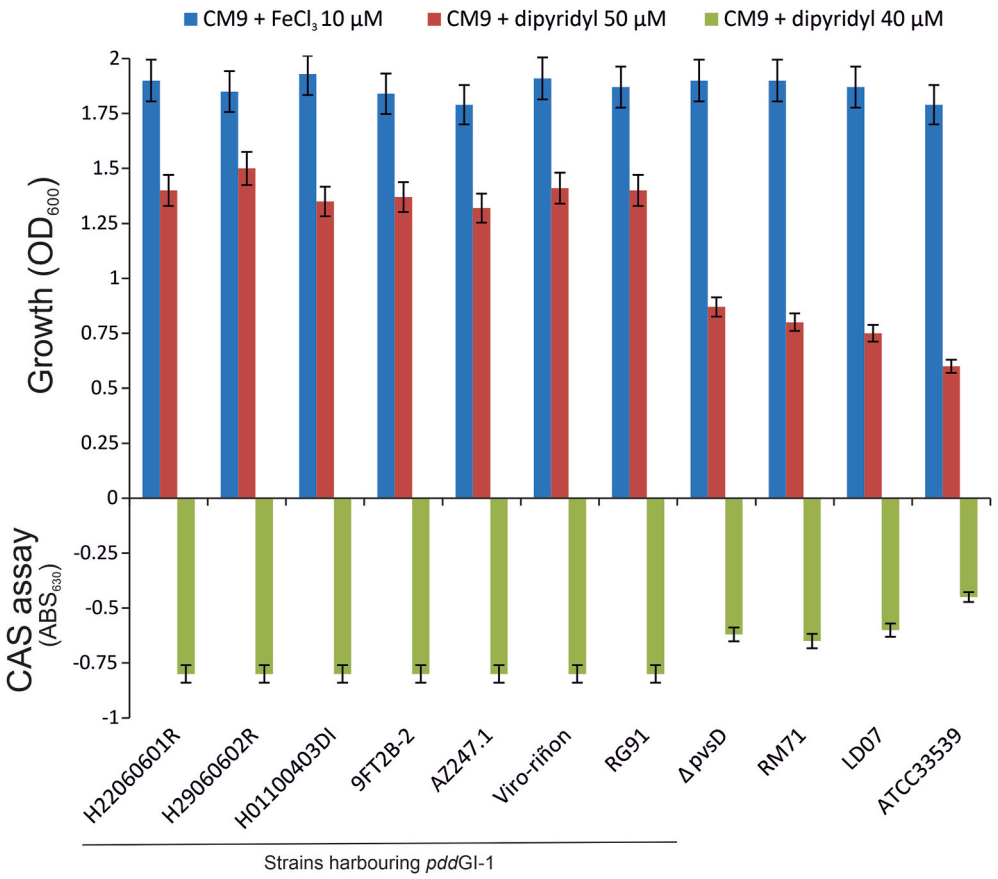

Fig. 4. Growth (OD_{600}) and siderophore production (CAS liquid assay) under iron-excess and iron-limited conditions by several *Pdd* strains harbouring *pdd*GI-1 compared with strains lacking this element.

3.6. Impact of vibrioferrin production on Pdd virulence

Turbot fingerlings were inoculated with either the RG91 parental strain or the RG91 *pvsD* mutant to evaluate the role of vibrioferrin in *Pdd* virulence. Both strains were pathogenic and capable of causing disease and death in turbot fingerlings (Fig. 5). After 10 days, survival rates were 60 % for fish inoculated with RG91 and nearly 80 % for those inoculated with the *pvsD* mutant (Fig. 5). Although the difference is statistically significant ($p < 0.05$), these results suggest that vibrioferrin production is not critical for the full virulence of RG91 in this experimental model. Further research is needed to better understand the role of vibrioferrin in *Pdd* virulence.

Iron acquisition is crucial for the successful colonization and invasion of many microbial pathogens [46]. However, the role of a specific siderophore in virulence depends on the strain's genetic background [51]. The RG91 *pvsD* mutant produces an alternative siderophore, which may compensate for the loss of vibrioferrin. Some *Pdd* strains can acquire iron from ferric citrate [19] and from heme and heme proteins in host tissues through mechanisms independent of siderophores [17]. Notably, when bacteria enter the host, genes for hemolysins (Dly and HlyA) and heme uptake are co-expressed, as their synthesis is induced under iron starvation conditions [14,17,20]. This suggests that in highly hemolytic *Pdd* strains, like RG91 [12], the combined effects of Dly and HlyA, along with the ability to utilize heme iron, may be sufficient to meet the bacterial iron needs within the host.

Bacterial pathogens often have multiple iron acquisition systems that may appear redundant in laboratory settings but serve specialized functions at the host-pathogen interface [52–54]. A key example is the *irp*-HPI genomic island encoding the siderophore piscibactin in *Vibrio anguillarum*, which has significant implications for bacterial adaptation to the host and pathogenesis, extending beyond iron uptake [55].

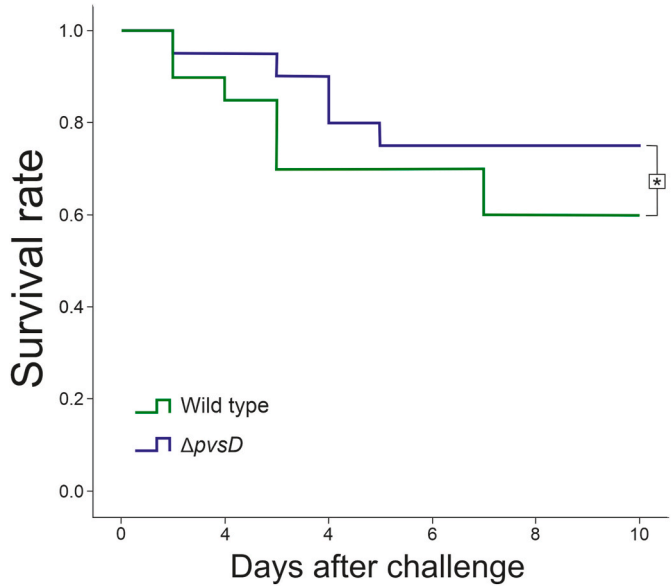

Fig. 5. Survival of turbot fingerlings (*Scophthalmus maximus*) inoculated with *Pdd* strains RG91 (parental) and *pvsD* defective mutant at 2×10^4 cells/fish. Fish mortality was recorded daily for 10 days after the pathogen IP injection. Asterisk denotes statistically significant differences ($P < 0.05$).

Siderophore systems are also crucial for understanding microbial population dynamics, as they play key roles in cooperation and competition for iron in natural bacterial communities [56,57]. This is particularly

true in marine environments, where vibrioferrin genes are widespread [45,47]. Therefore, the biological significance of vibrioferrin production in *Pdd* warrants further investigation.

4. Conclusions

Understanding genomic islands (GIs) is crucial for grasping bacterial evolution and identify potential virulence factors [58]. The *pdd*GI-1 element, a novel GI found in the highly virulent *Pdd* strain RG91, shares a common backbone with other well-characterized GIs in marine bacteria. PCR screening has revealed significant genome plasticity, affecting both the structure of *pdd*GI-1 and the genomic regions where these islands integrate. This indicates that *pdd*GI-1 may belong to a family of GIs prevalent in marine bacteria, contributing to their genetic diversity.

Our study shows that *pdd*GI-1 enables *Pdd* to produce vibrioferrin, which enhances growth under iron-limited conditions. Additionally, *pdd*GI-1 encodes potential fitness factors, such as defenses against foreign DNA and reactive oxygen species, as well as mechanisms for respiration under low-oxygen conditions. The role of these factors in bacterial fitness warrants further investigation.

While *pdd*GI-1 likely provides an advantage by expanding the genetic pool of *Pdd*, its direct contribution to virulence remains uncertain. The observed high levels of hemolysis and potential production of alternative siderophores might complement iron acquisition during fish infection. Our results also suggest that *Pdd* exhibits significant diversity in its iron acquisition mechanisms through siderophores.

CRediT authorship contribution statement

Beatriz Puentes: Visualization, Software, Methodology, Investigation, Data curation. **Alba Souto:** Writing – original draft, Visualization, Software, Methodology, Investigation, Data curation. **Miguel Balado:** Writing – original draft, Visualization, Methodology, Investigation, Formal analysis, Data curation, Conceptualization. **Jaime Rodríguez:** Writing – original draft, Visualization, Supervision, Software, Resources, Funding acquisition, Formal analysis, Data curation, Conceptualization. **Carlos R. Osorio:** Writing – review & editing, Supervision, Resources, Project administration, Funding acquisition, Formal analysis, Conceptualization. **Carlos Jiménez:** Writing – review & editing, Writing – original draft, Validation, Supervision, Resources, Project administration, Funding acquisition, Formal analysis, Conceptualization. **Manuel L. Lemos:** Writing – review & editing, Writing – original draft, Visualization, Supervision, Resources, Project administration, Funding acquisition, Formal analysis, Conceptualization.

Declaration of competing interest

The authors declare that they have no known competing financial interests or personal relationships that could have appeared to influence the work reported in this paper.

Acknowledgments

The work was supported by grants PID2021-122732OB-C21/C22 and PID2022-141987OB-I00 from MCIN/AEI/10.13039/501100011033/FEDER "A way to make Europe" (AEI, Spanish State Agency for Research and FEDER Programme from the European Union). M.B. was supported by grant PID2019-103891RJ-I00 from MCIN/AEI/10.13039/501100011033 (Spain). Work at the University of Santiago de Compostela and University of A Coruña was also supported by grants ED431C 2022/023 and ED431C 2022/39, respectively, from Xunta de Galicia, Spain.

Appendix A. Supplementary data

Supplementary data to this article can be found online at https://doi.org/10.1016/j.micpath.2024.107218.

References

[1] B. Austin, Vibrios as causal agents of zoonoses, Vet. Microbiol. 140 (2010) 310–317, https://doi.org/10.1016/j.vetmic.2009.03.015.
[2] A.J. Rivas, M.L. Lemos, C.R. Osorio, *Photobacterium damselae* subsp. *damselae*, a bacterium pathogenic for marine animals and humans, Front. Microbiol. 4 (2013) 283, https://doi.org/10.3389/fmicb.2013.00283.
[3] C.R. Osorio, A. Vences, X.M. Matanza, M. Terceti, *Photobacterium damselae* subsp. *damselae*, a generalist pathogen with unique virulence factors and high genetic diversity, J. Bacteriol. 200 (2018) e00002-18, https://doi.org/10.1128/jb.00002-18.
[4] A. Lozano-León, C.R. Osorio, S. Nuñez, J. Martínez-Urtaza, B. Magariños, Occurrence of *Photobacterium damselae* subsp. *damselae* in bivalve molluscs from Northwest Spain, Bull. Eur. Assoc. Fish Pathol. 23 (1) (2003) 40–44.
[5] T.-H. Chiu, L.-Y. Kao, M.-L. Chen, Antibiotic resistance and molecular typing of *Photobacterium damselae* subsp. *damselae* , isolated from seafood, J. Appl. Microbiol. 114 (2013) 1184–1192, https://doi.org/10.1111/jam.12104.
[6] P. Martins, D.F.R. Cleary, A.C.C. Pires, A.M. Rodrigues, V. Quintino, R. Calado, N. C.M. Gomes, Molecular analysis of bacterial communities and detection of potential pathogens in a recirculating aquaculture system for *Scophthalmus maximus* and *Solea senegalensis*, PLoS One 8 (2013) e80847, https://doi.org/10.1371/journal.pone.0080847.
[7] D.J. Grimes, P. Brayton, R.R. Colwell, S.H. Gruber, Vibrios as autochthonous flora of neritic sharks, Syst. Appl. Microbiol. 6 (1985) 221–226, https://doi.org/10.1016/S0723-2020(85)80056-4.
[8] J.D. Buck, R.S. Wells, H.L. Rhinehart, L.J. Hansen, Aerobic microorganisms associated with free-ranging bottlenose dolphins in coastal Gulf of Mexico and Atlantic ocean waters, J. Wildl. Dis. 42 (2006) 536–544, https://doi.org/10.7589/0090-3558-42.3.536.
[9] L. Serracca, C. Ercolini, I. Rossini, R. Battistini, I. Giorgi, M. Prearo, Occurrence of both subspecies of *Photobacterium damselae* in mullets collected in the river Magra (Italy), Can. J. Microbiol. 57 (2011) 437–440, https://doi.org/10.1139/w11-021.
[10] B. Fouz, J.L. Barja, C. Amaro, C. Rivas, A.E. Toranzo, Toxicity of the extracellular products of *Vibrio damsela* isolated from diseased fish, Curr. Microbiol. 27 (1993) 341–347, https://doi.org/10.1007/BF01568958.
[11] A. Labella, N. Sanchez-Montes, C. Berbel, M. Aparicio, D. Castro, M. Manchado, J. Borrego, Toxicity of *Photobacterium damselae* subsp. *damselae* strains isolated from new cultured marine fish, Dis. Aquat. Org. 92 (2010) 31–40, https://doi.org/10.3354/dao02275.
[12] A.J. Rivas, A.M. Labella, J.J. Borrego, M.L. Lemos, C.R. Osorio, Evidence for horizontal gene transfer, gene duplication and genetic variation as driving forces of the diversity of haemolytic phenotypes in *Photobacterium damselae* subsp. *damselae*, FEMS Microbiol. Lett. 355 (2014) 152–162, https://doi.org/10.1111/1574-6968.12464.
[13] A.J. Rivas, M. Balado, M.L. Lemos, C.R. Osorio, The *Photobacterium damselae* subsp. *damselae* hemolysins damselysin and HlyA are encoded within a new virulence plasmid, Infect. Immun. 79 (2011) 4617–4627, https://doi.org/10.1128/IAI.05436-11.
[14] A.J. Rivas, M. Balado, M.L. Lemos, C.R. Osorio, Synergistic and additive effects of chromosomal ($HlyA_{ch}$) and plasmid-encoded (Dly and $HlyA_{pl}$) hemolysins contribute to hemolysis and virulence in *Photobacterium damselae* subsp *damselae*, Infect. Immun. 81 (2013) 3287–3299, https://doi.org/10.1128/IAI.00155-13.
[15] A.J. Rivas, G. von Hoven, C. Neukirch, M. Meyenburg, Q. Qin, S. Füser, K. Boller, M.L. Lemos, C.R. Osorio, M. Husmann, Phobalysin, a small β-pore forming toxin of *Photobacterium damselae* subsp. *damselae*, Infect. Immun. 83 (2015) 4335–4348, https://doi.org/10.1128/IAI.00277-15.
[16] J.E. Cassat, E.P. Skaar, Iron in infection and immunity, Cell Host Microbe 13 (2013) 509–519, https://doi.org/10.1016/j.chom.2013.04.010.
[17] S.J. Río, C.R. Osorio, M.L. Lemos, Heme uptake genes in human and fish isolates of *Photobacterium damselae*: existence of *hutA* pseudogenes, Arch. Microbiol. 183 (2005) 347–358, https://doi.org/10.1007/s00203-005-0779-4.
[18] B. Fouz, E.G. Biosca, C. Amaro, High affinity iron-uptake systems in *Vibrio damsela*: role in the acquisition of iron from transferrin, J. Appl. Microbiol. 82 (1997) 157–167, https://doi.org/10.1111/j.1365-2672.1997.tb03568.x.
[19] M. Balado, B. Puentes, L. Couceiro, J.C. Fuentes-Monteverde, J. Rodríguez, C. R. Osorio, C. Jiménez, M.L. Lemos, Secreted citrate serves as iron carrier for the marine pathogen *Photobacterium damselae* subsp *damselae*, Front. Cell. Infect. Microbiol. 7 (2017) 361, https://doi.org/10.3389/fcimb.2017.00361.
[20] B. Puentes, M. Balado, J. Bermúdez Crespo, C.R. Osorio, M.L. Lemos, A proteomic analysis of the iron response of *Photobacterium damselae* subsp. *damselae* reveals metabolic adaptations to iron levels changes and novel potential virulence factors, Vet. Microbiol. 201 (2017) 257–264, https://doi.org/10.1016/j.vetmic.2017.01.040.
[21] M.S. Terceti, A. Vences, X.M. Matanza, I. Dalsgaard, K. Pedersen, C.R. Osorio, Molecular epidemiology of *Photobacterium damselae* subsp. *damselae* outbreaks in marine rainbow trout farms reveals extensive horizontal gene transfer and high genetic diversity, Front. Microbiol. 9 (2018) 2155, https://doi.org/10.3389/fmicb.2018.02155.
[22] M.L. Lemos, P. Salinas, A.E. Toranzo, J.L. Barja, J.H. Crosa, Chromosome-mediated iron uptake system in pathogenic strains of *Vibrio anguillarum*, J. Bacteriol. 170 (1988) 1920–1925, https://doi.org/10.1128/jb.170.4.1920-1925.1988.

[23] B. Schwyn, J.B. Neilands, Universal chemical assay for the detection and determination of siderophores, Anal. Biochem. 160 (1987) 47–56, https://doi.org/10.1016/0003-2697(87)90612-9.

[24] C.R. Osorio, A.J. Rivas, M. Balado, J.C. Fuentes-Monteverde, J. Rodríguez, C. Jiménez, M.L. Lemos, M.K. Waldor, A transmissible plasmid-borne pathogenicity island encodes piscibactin biosynthesis in the fish pathogen *Photobacterium damselae* subsp. *piscicida*, Appl. Environ. Microbiol. 81 (2015) 5867–5879, https://doi.org/10.1128/AEM.01580-15.

[25] S. Nurk, A. Bankevich, D. Antipov, A.A. Gurevich, A. Korobeynikov, A. Lapidus, A. D. Prjibelski, A. Pyshkin, A. Sirotkin, R. Stepanauskas, S.R. Clingenpeel, T. Woyke, J.S. McLean, R. Lasken, G. Tesler, M.A. Alekseyev, P.A. Pevzner, Assembling genomes and mini–metagenomes from highly chimeric reads, in: M. Deng, R. Jiang, F. Sun, X. Zhang (Eds.), Lecture Notes in Computer Science, 7821, Springer Verlag, Berlin Germany, 2013, pp. 158–170.

[26] R.K. Aziz, D. Bartels, A.A. Best, M. DeJongh, T. Disz, R.A. Edwards, K. Formsma, S. Gerdes, E.M. Glass, M. Kubal, F. Meyer, G.J. Olsen, R. Olson, A.L. Osterman, R. A. Overbeek, L.K. McNeil, D. Paarmann, T. Paczian, B. Parrello, G.D. Pusch, C. Reich, R. Stevens, O. Vassieva, V. Vonstein, A. Wilke, O. Zagnitko, The RAST Server: rapid annotations using subsystems technology, BMC Genom. 9 (2008) 75, https://doi.org/10.1186/1471-2164-9-75.

[27] S. Mouriño, C.R. Osorio, M.L. Lemos, Characterization of heme uptake cluster genes in the fish pathogen *Vibrio anguillarum*, J. Bacteriol. 186 (2004) 6159–6167, https://doi.org/10.1128/jb.186.18.6159-6167.2004.

[28] S. Yamamoto, N. Okujo, T. Yoshida, S. Matsuura, S. Shinoda, Structure and iron transport activity of vibrioferrin, a new siderophore of *Vibrio parahaemolyticus*, J. Biochem. 115 (5) (1994) 868–874, https://doi.org/10.1093/oxfordjournals.jbchem.a124432.

[29] T. Tanabe, T. Funahashi, H. Nakao, S.-I. Miyoshi, S. Shinoda, S. Yamamoto, Identification and characterization of genes required for biosynthesis and transport of the siderophore vibrioferrin in *Vibrio parahaemolyticus*, J. Bacteriol. 185 (2003) 6938–6949, https://doi.org/10.1128/JB.185.23.6938-6949.2003.

[30] T. Tanabe, H. Mitome, K. Miyamoto, K. Akira, H. Tsujibo, K. Tomoo, K. Nagaoka, T. Funahashi, Analysis of the vibrioferrin biosynthetic pathway of *Vibrio parahaemolyticus*, Biometals 37 (2) (2024) 507–517, https://doi.org/10.1007/s10534-023-00566-x. E.

[31] M. Dziejman, E. Balon, D. Boyd, C.M. Fraser, J.F. Heidelberg, J.J. Mekalanos, Comparative genomic analysis of *Vibrio cholerae*: genes that correlate with cholera endemic and pandemic disease, Proc. Natl. Acad. Sci. U.S.A. 99 (2002) 1556–1561, https://doi.org/10.1073/pnas.042667999.

[32] Y.A. O'Shea, S. Finnan, F.J. Reen, J.P. Morrissey, F. O'Gara, E.F. Boyd, The Vibrio seventh pandemic island-II is a 26.9 kb genomic island present in *Vibrio cholerae* El Tor and O139 serogroup isolates that shows homology to a 43.4 kb genomic island in V. vulnificus, Microbiol. 150 (2004) 4053–4063, https://doi.org/10.1099/mic.0.27172-0.

[33] H. Schmidt, M. Hensel, Pathogenicity islands in bacterial pathogenesis, Clin. Microbiol. Rev. 17 (2004) 14–56, https://doi.org/10.1128/CMR.17.1.14-56.2004.

[34] T.N. Farivar, P.J. Varnousfaderani, A. Borji, Mutation in alkylhydroperoxidase D gene dramatically decreases persistence of *Mycobacterium bovis* bacillus calmette-guerin in infected macrophage, Indian J. Med. Sci. 62 (2008) 275–282.

[35] D. Sambasivarao, J.H. Weiner, Dimethyl sulfoxide reductase of *Escherichia coli*: an investigation of function and assembly by use of in vivo complementation, J. Bacteriol. 173 (1991) 5935–5943, https://doi.org/10.1128/jb.173.19.5935-5943.1991.

[36] R.L. Jack, G. Buchanan, A. Dubini, K. Hatzixanthis, T. Palmer, F. Sargent, M. Alami, I. Luke, S. Deitermann, G. Eisner, H. Koch, J. Brunner, M. Müller, B. Berks, T. Palmer, F. Sargent, T. Bernhardt, P. de Boer, F. Blasco, J. Dos Santos, A. Magalon, C. Frixon, B. Guigliarelli, C. Santini, G. Giordano, N. Blaudeck, G. Sprenger, R. Freudl, T. Wiegert, K. Datsenko, B. Wanner, M. DeLisa, D. Tullman, G. Georgiou, A. Dubini, R. Pye, R. Jack, T. Palmer, F. Sargent, A. Dubini, F. Sargent, R. Gross, J. Simon, C. Hamilton, M. Aldea, B. Washburn, P. Babitzke, S. Kushner, K. Hatzixanthis, T. Palmer, F. Sargent, M. Ilbert, V. Mejean, M. Giudici-Orticoni, J. Samama, C. Iobbi-Nivol, M. Ilbert, V. Mejean, C. Iobbi-Nivol, R. Jack, F. Sargent, B. Berks, G. Sawers, T. Palmer, G. Karimova, J. Pidoux, A. Ullmann, D. Ladant, U. Lämmli, V. Mejean, C. Iobbi-Nivol, M. Lepelletier, G. Giordano, M. Chippaux, M. Pascal, I. Oresnik, C. Ladner, R. Turner, T. Palmer, F. Sargent, B. Berks, J. Pommier, V. Mejean, G. Giordano, C. Iobbi-Nivol, A. Rodrigue, A. Chanal, K. Beck, M. Müller, L. Wu, D. Sambasivarao, R. Turner, J. Simala-Grant, G. Shaw, J. Hu, J. Weiner, C. Santini, B. Ize, A. Chanal, M. Müller, G. Giordano, L. Wu, F. Sargent, E. Bogsch, N. Stanley, M. Wexler, C. Robinson, B. Berks, T. Palmer, S. Slepenkov, S. Witt, N. Stanley, F. Sargent, G. Buchanan, J. Shi, V. Stewart, T. Palmer, B. Berks, C. Temple, K. Rajagopalan, H. Towbin, T. Staehelin, J. Gordon, S. Tranier, C. Iobbi-Nivol, C. Birck, M. Ilbert, I. Mortier-Barriere, V. Mejean, J. Samama, S. Tranier, I. Mortier-Barriere, M. Ilbert, C. Birck, C. Iobbi-Nivol, V. Mejean, J. Samama, P. Vignais, A. Colbeau, Coordinating assembly and export of complex bacterial proteins, EMBO J. 23 (2004) 3962–3972, https://doi.org/10.1038/sj.emboj.7600409.

[37] C. Tseng, J. Albrecht, R. Gunsalus, Effect of microaerophilic cell growth conditions on expression of the aerobic (*cyoABCDE* and *cydAB*) and anaerobic (*narGHJI, frdABCD*, and *dmsABC*) respiratory pathway genes in *Escherichia coli*, J. Bacteriol. 178 (1996) 1094–1098, https://doi.org/10.1128/jb.178.4.1094-1098.199.

[38] A.K. Dunn, E.V. Stabb, Genetic analysis of trimethylamine N-oxide reductases in the light organ symbiont *Vibrio fischeri* ES114, J. Bacteriol. 190 (2008) 5814–5823, https://doi.org/10.1128/JB.00227-08.

[39] R.H. Kelly, P.H. Yancey, High contents of trimethylamine oxide correlating with depth in deep-sea teleost fishes, skates, and decapod crustaceans, Biol. Bull. 196 (1999) 18–25, https://doi.org/10.2307/1543162.

[40] R.J. Roberts, T. Vincze, J. Posfai, D. Macelis, REBASE–a database for DNA restriction and modification: enzymes, genes and genomes, Nucleic Acids Res. 38 (2009) D234–D236, https://doi.org/10.1093/nar/gkp874.

[41] M. Balado, M.L. Lemos, C.R. Osorio, Integrating conjugative elements of the SXT/R391 family from fish-isolated Vibrios encode restriction-modification systems that confer resistance to bacteriophages, FEMS Microbiol. Ecol. 83 (2013) 457–467, https://doi.org/10.1111/1574-6941.12007.

[42] A.M. Quirke, F.J. Reen, M.J. Claesson, E.F. Boyd, Genomic island identification in *Vibrio vulnificus* reveals significant genome plasticity in this human pathogen, Bioinformatics 22 (2006) 905–910, https://doi.org/10.1093/bioinformatics/btl015.

[43] T. Tanabe, H. Nakao, T. Kuroda, T. Tsuchiya, S. Yamamoto, Involvement of the *Vibrio parahaemolyticus pvsC* gene in export of the siderophore vibrioferrin, Microbiol. Immunol. 50 (2006) 871–876.

[44] T. Tanabe, T. Funahashi, N. Okajima, H. Nakao, Y. Takeuchi, K. Miyamoto, H. Tsujibo, S. Yamamoto, The *Vibrio parahaemolyticus pvuA1* gene (formerly termed *psuA*) encodes a second ferric vibrioferrin receptor that requires *tonB2*, FEMS Microbiol. Lett. 324 (2011) 73–79, https://doi.org/10.1111/j.1574-6968.2011.02389.x.

[45] O.X. Cordero, L.-A. Ventouras, E.F. DeLong, M.F. Polz, Public good dynamics drive evolution of iron acquisition strategies in natural bacterioplankton populations, Proc. Natl. Acad. Sci. U.S.A. 109 (2012) 20059–20064, https://doi.org/10.1073/pnas.1213344109.

[46] M. Miethke, M.A. Marahiel, Siderophore-based iron acquisition and pathogen control, Microbiol. Mol. Biol. Rev. 71 (2007) 413–451, https://doi.org/10.1128/MMBR.00012-07.

[47] K. Yarimizu, R. Cruz-López, E. García-Mendoza, M. Edwards, M.L. Carter, C. J. Carrano, Distribution of dissolved iron and bacteria producing the photoactive siderophore, vibrioferrin, in waters off Southern California and Northern Baja, Biometals 32 (1) (2019) 139–154, https://doi.org/10.1007/s10534-018-00163-3.

[48] S.A. Amin, D.H. Green, F.C. Küpper, C.J. Carrano, Vibrioferrin, an unusual marine siderophore: iron binding, photochemistry, and biological implications, Inorg. Chem. 48 (2009) 11451–11458, https://doi.org/10.1021/ic9016883.

[49] N. Castro, C.R. Osorio, N. Buján, J.C. Fuentes, J. Rodríguez, M. Romero, C. Jiménez, A.E. Toranzo, B. Magariños, Insights into the virulence-related genes of *Edwardsiella tarda* isolated from turbot in Europe: genetic homogeneity and evidence for vibrioferrin production, J. Fish. Dis. 39 (5) (2015) 565–576, https://doi.org/10.1111/jfd.12389.

[50] Z. Dumas, A. Ross-Gillespie, R. Kümmerli, Switching between apparently redundant iron-uptake mechanisms benefits bacteria in changeable environments, Proc. Biol. Sci. 280 (2013) 20131055, https://doi.org/10.1098/rspb.2013.1055.

[51] M. Smati, G. Magistro, S. Adiba, A. Wieser, B. Picard, S. Schubert, E. Denamur, Strain-specific impact of the high-pathogenicity island on virulence in extra-intestinal pathogenic *Escherichia coli*, Int. J. Med. Microbiol. 307 (2017) 44–56, https://doi.org/10.1016/j.ijmm.2016.11.004.

[52] J.D. Fetherston, O. Kirillina, A.G. Bobrov, J.T. Paulley, R.D. Perry, The yersiniabactin transport system is critical for the pathogenesis of bubonic and pneumonic plague, Infect. Immun. 78 (2010) 2045–2052, https://doi.org/10.1128/IAI.01236-09.

[53] K.S. Chaturvedi, C.S. Hung, J.R. Crowley, A.E. Stapleton, J.P. Henderson, The siderophore yersiniabactin binds copper to protect pathogens during infection, Nat. Chem. Biol. 8 (2012) 731–736, https://doi.org/10.1038/nchembio.1020.

[54] E.-I. Koh, J.P. Henderson, Microbial copper-binding siderophores at the host-pathogen interface, J. Biol. Chem. 290 (2015) 18967–18974, https://doi.org/10.1074/jbc.R115.644328.

[55] M.A. Lages, A. do Vale, M.L. Lemos, M. Balado, Remodulation of bacterial transcriptome after acquisition of foreign DNA: the case of *irp*-HPI high-pathogenicity island in *Vibrio anguillarum*, mSphere 9 (1) (2024) e0059623, https://doi.org/10.1128/msphere.00596-23.

[56] S.A. West, A. Buckling, Cooperation, virulence and siderophore production in bacterial parasites, Proc. R. Soc. B Biol. Sci. 270 (2003) 37–44, https://doi.org/10.1098/rspb.2002.2209.

[57] A.S. Griffin, S.A. West, A. Buckling, Cooperation and competition in pathogenic bacteria, Nat. 430 (2004) 1024–1027, https://doi.org/10.1038/nature02744.

[58] U. Dobrindt, B. Hochhut, U. Hentschel, J. Hacker, Genomic islands in pathogenic and environmental microorganisms, Nat. Rev. Microbiol. 2 (2004) 414–424, https://doi.org/10.1038/nrmicro884.